

14 AVR. 1986

TRI-PP-85-89  
Oct 1985

Measurement of the  $\pi^+ \rightarrow e\nu$  branching ratio

D.A. Bryman, \* M.S. Dixit, † R. Dubois, ‡ J.A. Macdonald, § T. Numa, §  
B. Olaniyi, ¶ A. Olin\* and J.-M. Poutissou||  
TRIUMF, Vancouver, B.C., Canada V6T 2A3 and  
National Research Council of Canada, Ottawa, Ont., Canada K1A 0R6

Abstract

A measurement of the  $\pi^+ \rightarrow e\nu$  branching ratio using a NaI(Tl) spectrometer yields a value  $\Gamma(\pi^+ \rightarrow e\nu + \pi^0 \nu) / \Gamma(\pi^+ \rightarrow \mu\nu + \pi^0 \nu) = (1.218 \pm 0.014) \times 10^{-4}$ . The result is consistent with expectations of the standard electroweak theory incorporating electron-muon universality.

(Submitted to Physical Review D)

CERN LIBRARIES, GENEVA



CM-P00067480

I. INTRODUCTION

The  $\pi^+ \rightarrow e\nu$  decay has long been of importance to the development of weak interaction theory. Early interest in the decay stemmed from its role in the confirmation of the (V-A) form of the universal Fermi interaction. As early as 1949, Ruderman and Finkelstein<sup>1</sup> had pointed out that a value of the branching ratio for  $(\pi^+ \rightarrow e\nu) / (\pi^+ \rightarrow \mu\nu)$  of about  $10^{-4}$  would indicate that the pion is a pseudoscalar particle and that  $\pi^2$  decay is governed by axial vector interactions. This assumed that the electron and the muon couple identically to the pion, an hypothesis now known as electron-muon ( $e-\mu$ ) universality in weak interactions. Under the assumption that the weak interaction contains only vector and axial vector terms, the branching ratio is given by

$$\frac{\Gamma(\pi^+ \rightarrow e\nu)}{\Gamma(\pi^+ \rightarrow \mu\nu)} = \frac{m_e^2 (m_\pi^2 - m_e^2)^2}{m_\mu^2 (m_\pi^2 - m_\mu^2)^2} = 1.28 \times 10^{-4}$$

where  $m_e c^2$ ,  $m_\mu c^2$  and  $m_\pi c^2$  are the electron, muon and pion masses, respectively, and the  $m_e^2/m_\mu^2$  helicity suppression term arises from the (V-A) form of the interaction. In contrast, for a pure pseudoscalar interaction the branching ratio would be  $(m_\pi^2 - m_e^2)^2 / (m_\pi^2 - m_\mu^2)^2 \sim 5 \cdot 4$ , and for other forms of couplings, the decay would be forbidden. After some initial difficulties, the decay was observed<sup>2</sup> in 1958 in agreement with the phenomenological (V-A) theory. With the subsequent establishment of the universal (V-A) theory,  $\pi^+ \rightarrow e\nu$  decay could be examined as a sensitive test of electron-muon universality.

In the framework of the Weinberg-Salam-Glashow (WSG) electroweak theory, Marciano and Sirlin<sup>3</sup> showed that the value of the  $\pi^+ \rightarrow e\nu$  branching ratio including radiative corrections is

IKI-PT 80-20  
C1

$$R = \frac{\Gamma(\pi \rightarrow e\nu + \pi + e\nu\nu)}{\Gamma(\pi \rightarrow \mu\nu + \pi + \mu\nu\nu)} = 1.233 \times 10^{-4}, \quad (1)$$

in close agreement with early calculations by Berman<sup>4</sup> and Kinoshita<sup>5</sup> and was a consequence of gauge invariance. Further, the additional pion structure dependent radiative corrections to R were no larger than 0.3%. This was confirmed in specific model calculations by Goldman and Wilson.<sup>6</sup> Thus, the  $\pi \rightarrow e\nu$  branching ratio provides a stringent test of  $e-\mu$  universality in the context of the standard electroweak theory. Although universality for the third generation lepton  $\tau$  is best constrained by agreement between the calculated and measured  $\tau$  lifetime,<sup>7</sup> the  $\pi \rightarrow e\nu$  branching ratio remains the most sensitive test of universality among the three known lepton generations.

In the quark sector three or more generations are necessary in order to accommodate CP violation in the standard model quark mixing matrix.<sup>8</sup> However, in the lepton sector there are still no compelling theoretical reasons for the existence of, or universality among the three generations;  $e-\mu$  universality is built-in and the lepton mixing matrix is diagonal due to the apparent masslessness of the neutrinos. Here, a search for rare lepton flavor-violating reactions such as  $\mu^- + \text{Nucleus} \rightarrow e^- + \text{Nucleus}$  or an accurate determination of the  $\pi \rightarrow e\nu$  branching ratio R can serve to probe the relationship between generations.

Deviations from the predicted branching ratio (1) would signal the presence of new physics. For example, the deviations could be due to small pseudoscalar terms<sup>9</sup> found in many extensions of the standard model which introduce new exotic particles. Because of interference between a pseudoscalar and the dominant axial vector terms, the  $\pi \rightarrow e\nu$  branching ratio is sensitive to terms proportional to  $M_H^{-2}$  where  $M_H$  is the mass

of the exotic particle that induces pseudoscalar terms in the interaction. This is in contrast with many still unobserved processes such as  $\mu \rightarrow e\nu$  for which the calculated rates are proportional to  $M_H^{-4}$ . Moreover, the sensitivity of the  $\pi \rightarrow e\nu$  decay for exhibiting exotic new effects is enhanced because of the natural helicity suppression of the standard model axial vector contribution relative to the pseudoscalar term.

Maximal helicity suppression is effective only in the case of massless neutrinos. If neutrinos were massive, the weak interaction eigenstates  $\nu_a$  could be admixtures of mass eigenstates  $\nu_i$  through a mixing matrix  $U_{ai}$ :

$$\nu_a = \sum U_{ai} \nu_i.$$

The  $\pi \rightarrow e\nu$  decay would then be an incoherent sum of decay modes  $\pi^+ \rightarrow e^+ \nu_i$ . The measured branching ratio R would be affected and additional peaks would appear in the  $\pi \rightarrow e\nu$  decay spectrum at energies determined by  $m(\nu_i)$  as emphasized by Shrock.<sup>10</sup> The sensitivity to branches involving massive neutrinos would be increased by about  $10^4$  relative to the zero mass neutrino case. Thus, the  $\pi \rightarrow e\nu$  decay is an experimentally favored reaction with which to search for the existence of massive neutrinos. The results of the search for massive neutrinos based on the present work in the mass range of 4 to 135 MeV have been described previously.<sup>11</sup>

The first accurate measurement of R was performed by Anderson et al.<sup>12</sup> in 1958 using a double focussing magnetic spectrometer. Positrons within a 10 MeV wide energy window extending up to the maximum  $\pi \rightarrow e\nu$  energy of 69.8 MeV were included to accept the inner bremsstrahlung radiative decays  $\pi \rightarrow e\nu\gamma$ . The measured branching ratio after correction for the unobserved low energy  $\pi \rightarrow e\nu\gamma$  positrons gave

$$R = (1.21 \pm 0.07) \times 10^{-4}$$

in agreement with the theoretical value Eq. (1).

In 1964 another measurement of R using a 23 cm diameter  $\times$  24 cm long NaI(Tl) crystal was reported by Di Capua et al.<sup>13</sup> With a correction<sup>14</sup> for a subsequently improved measurement of the pion lifetime, their result based on 10,000 events was

$$R = (1.274 \pm 0.024) \times 10^{-4}$$

This value of R was (3.3  $\pm$  1.9)% away from the theoretical value (1). A new measurement of the branching ratio with improved precision performed at TRIUMF<sup>15</sup> is described below in detail.

## II. EXPERIMENT

### A. Method

To measure the branching ratio R, the 69.8 MeV positrons from the  $\pi^+ \rightarrow e^+ \nu$  decay have to be detected in the presence of the  $10^4$  times more numerous positrons extending from 0-52.8 MeV that arise from the sequential decay process  $\pi \rightarrow \mu \nu$ , followed by  $\mu \rightarrow e \bar{\nu}$  (henceforth called the  $\pi$ - $\mu$ -e chain). A NaI(Tl) spectrometer is well suited to measure positrons over this wide energy range with good efficiency. The large  $\pi$ - $\mu$ -e chain component can be suppressed relative to  $\pi \rightarrow e \nu$  events by limiting observation to approximately one pion lifetime ( $\tau_{\pi} \sim 26$  ns) which is short compared to the muon lifetime ( $\tau_{\mu} \sim 2200$  ns). The decay time distribution can also be measured for both  $\pi \rightarrow e \nu$  and the  $\pi$ - $\mu$ -e chain events from which the  $\pi \rightarrow e \nu$  and  $\pi \rightarrow \mu \nu$  amplitudes can be obtained to calculate the branching ratio.

Using a method similar to that of Di Capua et al.,<sup>13</sup> energy spectra of positrons were collected during two identical time intervals, one

beginning at time  $t_1$  after the pion stop and the second beginning at time  $t_1 + t_0$  after the pion stop. The second interval essentially contained only positrons from the  $\pi$ - $\mu$ -e chain  $[N(2)_{\pi\mu e}]$  since  $t_0$  was long compared to the pion lifetime. However, the first interval contained events from both  $\pi$ - $\mu$ -e  $[N(1)_{\pi\mu e}]$  and  $\pi \rightarrow e \nu$   $[N_{\pi e}]$  origins. The branching ratio can then be expressed as:

$$R = \left( \frac{\lambda_{\mu}}{\lambda_{\pi} - \lambda_{\mu}} \right) \frac{N_{\pi e} \{1 - \exp[-(\lambda_{\pi} - \lambda_{\mu}) t_0]\}}{N(2)_{\pi\mu e} \exp\{\lambda_{\mu} t_0\} - N(1)_{\pi\mu e}} \quad (2)$$

where  $\lambda_{\pi}$  and  $\lambda_{\mu}$  are the pion and muon decay constants, respectively. This procedure to measure R is independent of several important sources of possible systematic uncertainties including the positron detector solid angle, the muon contamination of the beam, the displacement  $t_1$  of the beginning of the first measurement interval with respect to the pion stop, and absolute widths of the two time intervals (as long as they are identical).

In an alternative method to measure R, decay time distributions of positrons from  $\pi \rightarrow e \nu$  and the  $\pi$ - $\mu$ -e chain were measured from which amplitudes for the  $\pi \rightarrow e \nu$  and  $\pi \rightarrow \mu \nu$  components were obtained. The branching ratio is given by

$$R = \frac{A_{\pi \rightarrow e \nu}}{A_{\pi \rightarrow \mu \nu}} \quad (3)$$

### B. Setup

The experimental setup is shown in Fig. 1. Positive pions of momentum  $77 \pm 1$  MeV/c were produced by a 500 MeV, 100  $\mu$ A proton beam from the TRIUMF cyclotron striking a 1 cm long carbon target viewed by the M13 low energy pion channel. The beam was degraded by two plastic scintillation

beam counters B1 and B2 and stopped in the inner 3 layers of a five-element scintillation counter target (B3-B7) at a rate of  $2 \times 10^5 \text{ s}^{-1}$ . The inset of Fig. 1 shows the details of the stopping counter. The dimensions of the scintillation counters used in the experiment are given in Table I. The beam size at counter B1 was 2 cm x 2 cm. The muon and positron contamination in the beam were each 10%. Pions were selected by their range and by their time of flight ( $t_{fl}$ ) from the production target relative to a signal derived from the 23 MHz radiofrequency of the cyclotron which produced a  $\sim 3$  ns-wide beam burst on the pion production target every 43.4 ns. The pion stopping counters (B4, B5, and B6) were covered on the upstream and downstream sides by 150  $\text{mg}\text{-cm}^{-2}$  thick scintillators B3 and B3A and B7 and B7A, respectively, to retain the 4.2 MeV muons from pion decays in the target volume. The scintillator sections B3A and B7A were viewed by the same photomultipliers as B3 and B7, respectively. B8 was a large downstream counter used to veto beam particles which passed through the target.

A particle stopping in one of the three inner scintillators was defined by the logic B1.B2.B3.B4.( $\overline{\text{B7+B8}}$ ). A bit-pattern register, gated by the stop signal was used to determine in which scintillator the pion stopped (Fig. 2a). The range width of the stopping pions was 250  $\text{mg}\text{-cm}^{-2}$  (FWHM) with approximately 30%, 60% and 10% stopping in B4, B5 and B6, respectively. The positrons from the  $\pi + \text{ev}$  decay and from the  $\pi\text{-}\mu\text{-e}$  decay chain were detected by a three element scintillator telescope (T1, T2, T3) preceding the 46 cm diameter x 51 cm long NaI(Tl) crystal TINA at 90° with respect to the beam [see Fig. 1 and Table I]. T3 limited the positron solid angle acceptance to  $\Delta\omega/4\pi \approx 0.7\%$  so that the measurements

were confined to the central portion of the NaI(Tl) crystal to avoid edge effects and to obtain the best energy resolution.

The signal for a decay positron for the  $\pi + \text{ev}$  experiment was a T1.T2.T3 coincidence. To avoid energy dependence in the event trigger (especially at low energies) a signal from TINA was not required. As a result, the low energy end of the TINA spectrum contained two peaks — the zero energy pedestal and the 0.511 MeV positron annihilation gamma ray — due to the small fraction of triggers where the positron failed to register in the active volume of the NaI(Tl) crystal. During the early part of the experiment the decay positron detection arm also included three multiwire proportional chambers (MWPC) whose signals were not required in the logic. The MWPC data were used for offline analysis of position dependent systematic effects, multiple scattering, etc.

TINA was viewed by seven RCA4522 photomultipliers. Dynode outputs were passively added at the input of a charge sensitive preamplifier. The preamplifier signal was amplified and shaped with a 500 ns time constant and the pulse amplitudes were measured using a 4096 channel analog to digital converter (ADC). The tubes viewing the TINA crystal could be selectively removed from the analog sum to equalize gains by adjusting high voltages. The gains of the photomultipliers were monitored using the fitted positions of the zero energy pedestal, the 0.511 MeV annihilation line and the  $\mu\text{-e}\nu\bar{\nu}$  spectrum. For this purpose the muon decay positron spectrum was fitted to an empirical function

$$F(C) = \frac{a_1 + a_2C + a_3C^2 + a_4C^3}{1 + \exp[(C-a_5)/a_6]} \quad (4)$$

where C is the channel number,  $a_1$  to  $a_6$  are parameters with  $a_5$

corresponding to the Fermi half-amplitude energy and  $a_6$  being proportional to the resolution.

Figure 2b schematically shows the event logic. An event was accepted when there was a T1.T2.T3 coincidence within -160 to +230 ns of a pion stop. The energy losses ( $dE/dx$ ) in the scintillators T1 to T3 were also measured in order to identify positrons. An open ended delay line placed at the input of a discriminator triggered by the pion stop signal generated two identical 25 ns long time intervals hereafter called bin 1 and bin 2. Bits were set to flag events occurring during either of the two time bins.

Bin 1 started at  $t_1=3$  ns after the pion stop and bin 2 began  $t_s=173.4$  ns after  $t_1$  corresponding to 4 cyclotron rf periods or 6.7 pion lifetimes. The event time relative to the pion stop was measured using a time to amplitude converter and a 8192 channel ADC. The differential nonlinearity of the system was measured several times during the run, using a pulser in random coincidence with a source. The absolute time calibration was measured using the radiofrequency signal from the cyclotron as well as an Ortec 462 time calibrator, with a specified accuracy of  $\pm 0.005\%$ .

A beam pion preceding or following the current pion stop could disturb the measured time and energy spectra of the events (stop pileup). To detect stop pileup high threshold discriminators for the counters B1 and B3 were used (so as not to trigger the pileup logic with beam or decay positrons). The pileup signal was triggered by B1 or (B3.T2). The B3.T2 requirement was imposed in order to recover events for which the decay positron produced a large pulse in counter B3 due to the Landau fluctuations in the positron energy loss. Arrival time of pileup

particles was measured with a TDC if there was a beam pion within  $\pm 5$   $\mu$ s of the current stop. In addition, a bit was set in a register for pileup of beam pions within  $\pm 325$  ns of the pion stop.

The TINA energy spectrum could be distorted by additional charged particles close in time to the event (TINA pileup). Counter T2 was used to record the charged particle pileup arrival time in TINA within  $\pm 5$   $\mu$ s of the event. Figure 2c shows schematically the stop pileup and the TINA pileup logic. Figure 3a and 3b show the time distributions and the timing logic sequence for all events.

The data were recorded event-by-event via CAMAC by a PDP11/34A computer. The following information was recorded for each event:

- a) Scintillator bit patterns
- b) Time of the event relative to the stop
- c) NaI(Tl) pulse height for the event
- d) Beam pion pileup times relative to the pion stop within  $\pm 5$   $\mu$ s. (Stop pre- and post-pileup).
- e) T2 charged particle pileup time relative to the event within  $\pm 5$   $\mu$ s. (TINA pre- and post-pileup).
- f) Energy loss information for the scintillators T1, T2, and T3.
- g) MWPC 1-3 data.

**C. Line shape measurement**

Detailed knowledge of the NaI(Tl) spectrometer response function, including resolution, peak shape, and magnitude of the characteristic low energy tail, was essential to the data analysis. The response functions were measured separately in a positron beam with momentum spread of  $\Delta p/p = 1\%$  at 20, 35, 50, 70, and 90 MeV/c. The positron beam was

defocussed and events were accepted with a radius of 5 cm from the crystal axis corresponding to the acceptance of the T3 counter in the  $\pi^+e\nu$  experiment. The energy resolution at 70 MeV/c was  $\Delta E/E = 3.5\%$  (FWHM). Over the measured energy range, the FWHM width,  $\Gamma$ , could be well represented by

$$\Gamma(\%) = 46.3 E^{-0.5745}, E \text{ in MeV} . \quad (5)$$

The fractional number of counts in the tail portion of the line shapes corresponding to the region of the  $\pi^+e\nu$  peak lying below the  $\mu^+e\nu$  edge was measured at different energies. The result was characterized by an uncertainty of 0.55% due in part to a small contamination of pions and muons in the positron beam for the 70 and 90 MeV/c measurements.

Figure 4 shows the measured NaI response function for the 50 MeV/c case.

### III. DATA REDUCTION

To produce a data set suitable for the branching ratio calculation a number of cuts had to be applied to the raw data.

#### A. Stop prepileup cut

This cut eliminated those events for which there was a beam particle within a given interval prior to the  $\pi$  stop which triggered the event. Since the  $\mu$  lifetime is long compared to the  $\pi$  lifetime, increasing the length of the protection interval reduced both the relative number of  $\mu^+e\nu$  decay events from previous  $\pi$  stops and the total number of events. The prepileup cut chosen was 525 ns, a compromise between maximizing the total  $\pi^+e\nu$  event rate and minimizing the  $\mu^+e\nu$  events from previous pion stops.

#### B. Stop postpileup cut

The decays of pions which arrived at the target after the trigger stop but within the event acceptance window distorted the shape of the

timing spectra. They also produced additional events in bin 2. The probability of a beam pion appearing in the event time window following the trigger stop was 3.5%. The bit set for additional beam pions within  $\pm 325$  ns of the trigger stop was used to discriminate against stop postpileup events. The efficiency of this cut was studied for its effect on the branching ratio determination.

#### C. Event $dE/dx$ cut

Beam pions caused emission of prompt protons via  $^{12}\text{C}(\pi^+,p)\text{X}$  reactions primarily in the B1 counter. The observed prompt proton energy spectrum extended to about 90 MeV and these events could distort the energy and time distribution of events. Protons were easily distinguished by their high  $dE/dx$  compared to the minimum ionizing positrons. The  $dE/dx$  information from the three scintillators T1, T2 and T3 was combined to produce a nearly gaussian energy loss spectrum using the minimum pulse theory.<sup>16</sup> The prompt proton cut applied in this way was estimated to eliminate less than 0.1% of the  $\pi^+e\nu$  events.

#### D. TINA charged particle prepileup and postpileup

Additional charged or neutral particles entering the NaI(Tl) crystal before or after the event positron caused energy resolution degradation due to pulse pileup. The pileup cut for charged particles was derived from the T2 scintillator covering the entire front face of the crystal. No improvement in the resolution was noted for values of prepileup and postpileup protection intervals larger than 1.5  $\mu\text{s}$  and the cut was set at this value. A small correction to the  $\pi^+e\nu$  branching ratio which resulted from this cut is described in Sec. IV B.

#### E. Gain correction

A gain correction for signals from TINA was made before obtaining an absolute energy calibration. The relative gain of each run was calculated using the positions of the two low energy peaks fitted to Gaussians and the  $\mu$ - $e\nu$  energy spectrum fitted to the empirical function of Eq. (4). The gain stability over a 2 month running period was  $\pm 2\%$ . The energy spectra from individual runs were gain shifted to a standard gain to produce the summed bin 1 and bin 2 energy spectra needed to obtain the tail corrections and to calculate the branching ratio using the two bin method. Branching ratios were also calculated for the individual runs without gain shifting as a check of consistency and rate effects. These were found to be in good agreement with the value obtained from the gainshifted sum.

Gainshifted data were also used to produce timing spectra for  $\pi + e\nu$  events above a 52.9 MeV cutoff energy and for  $\mu + e\nu$  events below this energy. These spectra were used in the second calculation of the branching ratio using the timing fits.

#### IV. DATA ANALYSIS AND RESULTS

##### A. Energy calibration and tail correction

Energy calibration required detailed analysis of bin 1 and bin 2 energy spectra. Figure 5(a) shows the spectrum of positron energy deposited in the NaI(Tl) crystal for bin 1 including the  $\pi + e\nu$  peak and the  $\mu + e\nu$  spectrum. It extends to zero observed energy since the NaI(Tl) pulse was not required in the event logic. The expanded low energy region shown in Fig. 5(b) reveals the two low-energy peaks due to the zero-energy ADC pedestal and the 0.511 MeV positron annihilation line. These two peaks were due to positrons which stopped in T3 or in

the insensitive front layer of TINA consisting of 1.6 mm of Al, 0.3 mm  $\text{CH}_2$ , and 1.6 mm of packed MgO (reflective layer). Figure 5(c) gives the pure  $\mu + e\nu$  spectrum from bin 2.

To obtain the branching ratio the number of  $\pi$ - $\mu$ - $e$  events in bins 1 and 2 and the total number of  $\pi + e\nu$  events in bin 1 are required. For the  $\pi + e\nu$  events a correction must be made for the small fraction of events which fall under the  $\pi$ - $\mu$ - $e$  spectrum due to radiative processes, to the NaI(Tl) resolution function with its characteristic low energy tail, and to energy loss for the beam-target-detector geometry. Since the tail correction corresponded to approximately 1.5% of the total number of  $\pi + e\nu$  events below 51 MeV it was crucial to calculate it precisely. This calculation relied on the detailed knowledge of the NaI line shape for the  $\pi$ - $e\nu$  events and on the energy calibration. Both were obtained by using Monte Carlo generated empirical  $\pi + e\nu$  and  $\mu + e\nu$  line shapes.

Figure 6 shows the experimental  $\pi + e\nu$  bin 1 spectrum obtained by subtracting the normalized bin 2  $\mu + e\nu$  spectrum from bin 1. Also shown is the fit to the data using the Monte Carlo generated  $\pi + e\nu$  line shape. The  $\chi^2$  is 1.01 per degree of freedom indicating that no important effects have been overlooked. The measured peak width of  $\Delta E/E=5.5\%$  is in agreement with the Monte Carlo calculation. There are  $N_{\pi e} = 3.2 \times 10^4$  counts in the peak with  $E > 51$  MeV.

To determine the empirical  $\pi + e\nu$  Monte Carlo line shape, pions were simulated to stop in the target according to the measured range curve (FWHM=250  $\text{mg-cm}^{-2}$  centred 60  $\text{mg-cm}^{-2}$  upstream of the target center). For the experimental geometry,  $\pi + e\nu$  decay positrons were traced from the target to the NaI(Tl) crystal allowing for  $\pi + e\nu$  inner bremsstrahlung radiative corrections,<sup>17</sup> Landau energy loss fluctuations and Bhabha

scattering. The total energy deposited in the crystal was obtained by summing the kinetic energy of the detected positron, positron annihilation energy (1.02 MeV) and the energies of any detected radiative photons and Bhabha scattered electrons. This energy spectrum was then numerically convoluted with the measured crystal resolution functions using Eq. (5) for interpolation to produce the empirical  $\pi \rightarrow e\nu$  line shape used to fit the experimental  $\pi \rightarrow e\nu$  data.

The empirical shape for the  $\mu \rightarrow e\nu\bar{\nu}$  spectrum was obtained from a Monte Carlo calculation similar to the one for the  $\pi \rightarrow e\nu$  events. Pions stopped in the target according to the measured range curve. The 4.2 MeV muons from the pion decay were contained in the target region and were allowed to decay into electrons. As with  $\pi \rightarrow e\nu$  events, a spectrum containing the various simulated physical processes was produced including  $\mu \rightarrow e\nu\bar{\nu}$  radiative corrections<sup>18</sup> for the experimental geometry. This line shape was convoluted with the measured NaI(Tl) resolution functions to produce the empirical Monte Carlo  $\mu \rightarrow e\nu\bar{\nu}$  spectrum shape.

Acceptable fits to both the bin 1 and bin 2  $\mu \rightarrow e\nu\bar{\nu}$  spectra could only be obtained by excluding the pileup region above 49 MeV and the low energy region below 5 MeV where the energy loss and resolution uncertainties were large. The fit provided adequate energy information for the  $\mu \rightarrow e\nu\bar{\nu}$  spectrum needed for energy calibration. The energy calibration of the data, given in Table II, was obtained by making a least squares fit to the  $\pi \rightarrow e\nu$  peak, the  $\mu \rightarrow e\nu\bar{\nu}$  spectrum and the two low energy peaks. The branching ratio determination was insensitive to the distortions in the  $\mu \rightarrow e\nu\bar{\nu}$  spectrum since only the total number of counts is used as discussed below.

An estimate for the magnitude of the two low energy peaks including the effects of multiple scattering gave  $(0.55 \pm 0.20)\%$  of the total number of counts in the  $\mu \rightarrow e\nu\bar{\nu}$  spectrum. This was in good agreement with the measured values of  $(0.725 \pm 0.004)\%$  and  $(0.710 \pm 0.003)\%$  for bins 1 and 2 respectively. The small excess of counts in the low energy peaks in bin 1 over bin 2 has been estimated to be due to Compton scattering of the  $\gamma$ 's from  $\pi \rightarrow \mu\nu$  decays in the target material.

**B. Branching ratio using the two bin method**

The total number of  $\pi \rightarrow e\nu$  events was obtained by calculating the number of events above a cutoff energy  $E_c$  and applying a tail correction below this energy using the Monte Carlo generated line shape. In order to assess the reliability of the tail correction, it was calculated as a function of  $E_c$ . The stability of the branching ratio obtained as  $E_c$  was varied indicated the validity of the tail correction. The energy spectrum was divided into the  $\pi \rightarrow e\nu$  region above  $E_c$  and the  $\mu \rightarrow e\nu\bar{\nu}$  region below  $E_c$ . A fraction,  $p$ , of the  $\pi \rightarrow e\nu$  counts were below  $E_c$  due to the tail of the  $\pi \rightarrow e\nu$  line shape and a fraction,  $q$ , of the  $\mu \rightarrow e\nu\bar{\nu}$  counts were above  $E_c$  due to pileup effects in the energy spectra. We further defined for the two bins ( $i=1,2$ ) total  $\pi \rightarrow e\nu$  region counts  $n_i$ , total  $\pi \rightarrow \mu\text{-e}$  region counts  $m_i$ , net  $\pi \rightarrow e\nu$  counts  $a_i$  and net  $\pi\text{-}\mu\text{-e}$  counts  $b_i$ , with  $\lambda_\pi$ ,  $\lambda_\mu$  and  $t_s$  having been defined earlier (Sec. IIA). It can be shown that

$$a_i = (m_2 n_1 - m_1 n_2) / [m_2(1-p) - p n_2 e^{-\lambda_\pi t_s} \{m_1(1-p) - n_1 p\}] \quad (6)$$

$$b_i = n_1 + m_1 - a_i \quad (7)$$

$$b_2 = n_2 + m_2 - a_2 e^{-\lambda_\pi t_s} \quad (8)$$

Then the tail corrected branching ratio becomes



$$R_1 = \frac{a_1}{e^{\lambda_\mu t_g} b_2 - b_1} \frac{\lambda_\mu}{\lambda_\pi - \lambda_\mu} \left[ 1 - e^{-t_s(\lambda_\pi - \lambda_\mu)} \right]. \quad (9)$$

There are two conflicting requirements in applying the tail corrections. Ideally  $E_c$  should be as low as possible in order to apply the least correction. Unfortunately, lowering  $E_c$  increases the  $\mu + e\bar{\nu}$  contamination to be subtracted from under the  $\pi + e\nu$  events leading to increased statistical uncertainty. A compromise was reached at  $E_c=51$  MeV from these considerations and the stability of the branching ratio as a function of  $E_c$ . The uncertainty in the tail correction due to the choice of the cutoff energy was estimated to be 0.51%. When combined with the earlier uncertainty of 0.55% in the measured  $\text{NaI(Tl)}$  resolution function, this led to a total uncertainty of 0.75%. The overall tail correction applied to the branching ratio was  $(1.47 \pm 0.75)\%$ .

Several other corrections shown in Table III were applied to the tail corrected branching ratio to obtain the final branching ratio. These were obtained from Monte Carlo calculations or from detailed analysis of data. The accuracy in evaluation of these corrections is affected by the uncertainties in the geometry for the target, scintillators and the  $\text{NaI(Tl)}$  detector. These corrections are discussed below.

After the tail correction, effects of multiple scattering led to the next largest uncertainty. Multiple Coulomb scattering is an energy dependent process in which positrons may be scattered into or out of the acceptance. A Monte Carlo simulation based on Moliere theory corrected<sup>19</sup> for finite scattering angles ( $\sin\theta \neq 0$ ) was done. As a check the calculation reproduced existing precise measurements of multiple scattering of low energy electrons in gold and beryllium.<sup>20</sup> For the  $\pi + e\nu$  and  $\mu + e\bar{\nu}$  events the program kept track of the number of particles

scattered into or out of the acceptance. Calculations were repeated for variations in the beam-target-detector geometry to determine the effect of uncertainties in the geometry. From these calculations a multiplicative correction factor due to multiple scattering of  $0.9977 \pm 0.0040$  for the branching ratio was obtained.

Some of the positrons annihilated in the scintillators before reaching the  $\text{NaI(Tl)}$  crystal. The energy dependent annihilation cross section was taken from Heitler.<sup>21</sup> The difference in the annihilation for  $\pi + e\nu$  events and  $\mu + e\bar{\nu}$  events led to a multiplicative correction factor of  $(0.9959 \pm 0.0010)$  for the branching ratio. Some of the low energy positrons from the  $\mu + e\bar{\nu}$  decay were lost from the trigger due to low range. These led to a trigger loss correction factor of  $0.9982 \pm 0.0005$ .

The branching ratio determination depends on precise equality of the two time bins. A measurement of the two bin widths by counting a radioactive source in random coincidence with a pulser indicated a small difference which led to a branching ratio correction of  $(0.9989 \pm 0.0004)$ . The 100 ps uncertainty in the measured bin separation  $t_g$  had a negligible effect on the branching ratio.

There were three small corrections required to account for aspects of the target configuration. A factor of  $(0.9986 \pm 0.0011)$  accounted for the effect of a difference in solid angle for  $\mu + e\bar{\nu}$  events and  $\pi + e\nu$  events due to the fact that the 4.2 MeV decay muons occupy a slightly larger volume in the target than the original pions. Although it was determined that all the decay muons from stopped pions were contained within the total target volume, it was possible for a fraction of pions to decay to muons which entered the veto counter B7. The

resulting false stop veto signals caused a small loss of stops and required a correction factor of  $(1.0002 \pm 0.0010)$ . Parts of the last segment of the target (B/A lip - see Fig. 1) could intercept a fraction of the solid angle for positrons from both  $\pi^+ + e\nu$  and  $\mu^+ + e\nu$  decay. At early time ( $< 10$  ns) this could lead also to lost events due to a false stop veto in the target. The correction for this was  $(1.0018 \pm 0.0017)$ .

The effects of the pileup cuts on the branching ratio were determined by using different sets of pileup conditions in the analysis and from measured inefficiencies of the counters. The following effects were included.

- i) Inefficiencies in the detection of stop post pileup.
- ii) A small distortion in the bin 1 and bin 2 event ratio due to the fact that the rate of TINA pileup depended on the counter T2 rate which varied with time after the pion stop.
- iii) A fraction of the stop post pileup signals were false because they were generated by a stopped pion in counter B4 that decayed into a muon which could enter the active volume of counter B3 and trigger the post pileup logic.

The resulting overall correction factor from the pileup effects was  $(0.9931 \pm 0.0029)$ . Finally, the uncertainty in the measured pion lifetime<sup>22</sup>  $\tau_\pi = 1/\lambda_\pi = 26.030 \pm 0.023$  ns contributed a correction factor of  $1.0000 \pm 0.0069$  to the branching ratio.

Including the corrections listed in Table III the final value of the branching ratio based on the data shown in Fig. 5 and Eq. (9) is

$$R = (1.218 \pm 0.014) \times 10^{-4} \quad (10)$$

### C. Branching ratio using the timing method

The second method for determining the branching ratio made use of the data shown in the two timing spectra in Fig. 7. Events which occurred prior to the arrival of the pion ( $t=0$ ) were due to decays of muons left in the target by previous pion stops. The time distributions included all events in the  $\pi^+ - \mu^+ - e$  energy region (Fig. 7a) and in the  $\pi^+ + e\nu$  peak region (Fig. 7b) over a wider time range than just bins 1 and 2.

The full expression used to fit the timing spectra included a muon contamination in the pion beam and small corrections to account for the effects of the pileup circuitry. The function for events below  $E_c = 52.9$  MeV due mostly to the  $\pi^+ - \mu^+ - e$  decay chain was:

$$f_{\pi^+e}(t) = N \left[ \theta(t) \left\{ (1-q-R) \cdot \phi(t) + R p \lambda_\mu e^{-\lambda_\mu t} + a_1 \lambda_\mu e^{-\lambda_\mu t} \right\} - \theta(t-t_F) \cdot a_2 \cdot \phi(t-t_F) + \sum_{n \neq 0}^8 \theta(t-t_{rF}^n) \phi(t-t_{rF}^n) a_3 + a_4 \lambda_\mu e^{-\lambda_\mu t} \right], \quad (11)$$

The expression for  $\pi^+ + e\nu$  decay events above the cutoff energy  $E_c$  was:

$$f_{\pi^+e}(t) = N \left[ \theta(t) \left\{ R \cdot (1-p) \lambda_\pi e^{-\lambda_\pi t} + q \phi(t) \right\} + a_3 \cdot R \cdot \sum_{n \neq 0}^8 \theta(t-t_{rF}^n) \lambda_\pi e^{-\lambda_\pi (t-t_{rF}^n)} + a_5 \lambda_\mu e^{-\lambda_\mu t} \right], \quad (12)$$

where  $\theta(t)=0$  for  $t < 0$  ns and  $\theta(t)=1$  otherwise.

Here N is the total number of pion decays, R the branching ratio to be determined and the function  $\phi(t)$  describes the sequential  $\pi^+ - \mu^+ - e$  decay chain time distribution,

$$\phi(t) = \frac{\lambda_{\pi} \lambda_{\mu}}{\lambda_{\pi} - \lambda_{\mu}} (e^{-\lambda_{\mu} t} - e^{-\lambda_{\pi} t}) .$$

The tail of the NaI(Tl) response function caused a fraction  $p$  of the  $\pi + \text{ev}$  counts below  $E_C$  to be included in the function  $f_{\pi\mu e}(t)$ .

Similarly, resolution and pileup effects in the energy spectrum caused a fraction  $q$  of  $\pi-\mu-e$  events above  $E_C$  to be included in the function  $f_{\pi e}(t)$ . The parameter  $\alpha_1$  accounted for the muon component in the beam.

Pileup effects were explicitly included in the fitting functions. A fraction  $\alpha_2$  of the pions stops in the counter B4 could decay to muons stopping in B3 and caused a false stop pileup. The retrigging time for this process was  $t_{\text{tr}} \sim 28$  ns.

The terms with  $\alpha_3$  accounted for the inefficiency of the stop pileup circuitry for beam pions in the subsequent rf cycles spaced  $t_{\text{rf}} = 43.4$  ns apart. The  $\alpha_4$  and  $\alpha_5$  terms accounted for muon decays from previous pions stopping before the pre-pileup cut of 525 ns (Sec. III A).

In addition, two small corrections (not indicated in Eq. 11 and 12) arising from events incorrectly vetoed by the edge of counter B7 (B7A lip veto) and TINA pileup correction were introduced into both  $\pi-\mu-e$  and  $\pi + \text{ev}$  time spectra. The multiplicative correction term from the B7A lip veto is  $h(t) = 0.999$  for  $-7 \text{ ns} \leq t \leq 7 \text{ ns}$  and  $h(t) = 1.000$  otherwise, applied to  $f_{\pi\mu e}$  and  $f_{\pi e}$ . The effect of TINA pileup required a correction factor of  $(1 - 0.004e^{-\lambda_{\mu} t})$  for the  $\pi + \text{ev}$  and  $\pi-\mu-e$  components. The correction factor was  $(1 + 0.03e^{-\lambda_{\mu} t})$  for the muons. [See pileup corrections Section IV B].

The timing spectra of  $\pi-\mu-e$  and  $\pi-\text{ev}$  events were fitted simultaneously using a fitting program, MINUIT.<sup>23</sup> Free parameters were the

number of  $\pi$  decay events  $N$ , the muon decay terms  $\alpha_4$  and  $\alpha_5$ , the branching ratio  $R$ , the fraction  $q$  of  $\pi-\mu-e$  events above  $E_C$ , and the zero time ( $t_0$ ) which was introduced by replacing  $t-t_0$  for  $t$  in Eq. (11) and (12).

The  $\pi$  and  $\mu$  lifetimes were set at the currently accepted values of 26.03 ns and 2197.3 ns, respectively. The tail correction  $p$  for  $\pi-\text{ev}$  events below  $E_C$  was set at 0.021 as determined from the line shape analysis.

The amplitude arising from the  $\mu$  contamination in the beam,  $\alpha_1$ , was set to be zero based on an estimation of  $<0.3\%$  from the TOF spectrum of the incident particles for the analysed events. Based on separate analysis, the B3 false stop pileup correction  $\alpha_2$  was fixed at  $-0.00475$  and the stop pileup inefficiency correction  $\alpha_3$  was set at 0.00024 which is a product of the measured inefficiency of the scintillators and the probability of having random incident particles. Errors due to uncertainties in the fixed parameters were estimated by varying each parameter and are included in Table IV.

To estimate systematic effects, a term with time dependence  $e^{-2\lambda_{\mu} t}$  was introduced as additional background. Terms with this time dependence arise in second order from TINA pileup corrections. A small but statistically significant component with this time dependence was found, and about 20% of it could be accounted for from the TINA pileup correction. The source of the remainder is unknown. The introduction of this component led to an increase of 0.3% in the branching ratio.

In the study of systematic effects, several fixed parameters were also set free in the fits. The maximum variation of the branching ratio was 0.4% which happened when the B3 false stop pileup converged to  $\alpha_3 = 0.0001$ . The difference of the branching ratio between the fits with free and fixed pion lifetime was 0.1%. The dependence on the fitting

region was studied by varying the regions for the fit. This resulted in an uncertainty of 0.3% in the branching ratio. Close inspection of Fig. 7(a) shows an anomalous distortion in the time region near 120 ns. The difference between the values of R calculated including and excluding the anomalous distortion (wiggle) region was about 0.1%. The  $\chi^2/DF$  was 1.6 when the wiggles were in the fit and 1.2 when they were excluded. An uncorrected branching ratio of  $(1.231 \pm 0.007) \times 10^{-4}$  was obtained when the fitting region was from -130 ns to 180 ns excluding the time zero region (-40 ns to ~5 ns) and the definite wiggle regions.

In addition to the fitting procedure certain of the multiplicative corrections determined for the two bin method (section IV B) must be applied to the result. The corrections applicable, listed in Table IV are low energy  $\pi$ - $\nu$ e trigger losses, pion-muon solid angle difference,  $\pi$ - $\nu$  decay false veto in the target, multiple scattering and positron annihilation. Including all the above corrections, the branching ratio determined from the timing method is

$$R = (1.219 \pm 0.014) \times 10^{-4} \quad (14)$$

and is consistent with the result of Eq. (10).

#### D. Pion Lifetime

During the validity test of the expression for the timing fit, a pion lifetime was deduced from the same spectrum that was used in the study of the branching ratio. When the pion lifetime was left as a free parameter in the fit a value of  $26.10 \pm 0.05$  ns including only a statistical error, was obtained in good agreement with the currently accepted value<sup>22</sup> of  $26.030 \pm 0.023$  ns. This helps to confirm the validity of the fitting expression. To estimate the systematic uncertainties in this number, the effect of uncertainties in the other parameters was studied

by varying their values. Since the timing spectrum around  $t_0$  ( $\pi$  stop) was disturbed by the introduction of pileup cuts (a typical example is the B3 stop pileup), there seems to be a slight dependence on the fitting region. This was also true in the determination of the branching ratio as mentioned in the previous section. The uncertainty due to different fitting regions was estimated to be 0.11 ns from the fits for different regions. The error from the uncertainty of the B3 false pileup was 0.04 ns. The contributions from other fixed parameters, such as the muon contamination in the beam, were negligible. The pion lifetime obtained by combining these uncertainties in quadrature is  $26.10 \pm 0.13$  ns.

#### V. CONCLUSIONS

The result for the branching ratio of Eq. (10) (or Eq. (14)) is in good agreement with the predictions of the standard model of weak and electromagnetic interactions with the assumption of electron-muon universality. A quantitative test of universality can be obtained by writing Eq. (1) as

$$R = 1.233 (f_{\pi}^e/f_{\pi}^{\mu})^2 \times 10^{-4} = (1.218 \pm 0.014) \times 10^{-4} \quad (14)$$

where  $f_{\pi}^e$  is the pion decay constant. Then

$$f_{\pi}^e/f_{\pi}^{\mu} = 0.9939 \pm 0.0057 \quad (15)$$

where a value of unity corresponds to perfect universality. This test of  $e$ - $\mu$  universality is unaffected by the uncertainty in the  $\pi \rightarrow e\nu$  branching ratio due to pion structure dependent effects.<sup>24</sup>

The branching ratio is very sensitive to the contribution of a pseudoscalar coupling to  $\pi_{L2}$  decay because decays via this mechanism are not helicity-suppressed. The resulting limit on the pseudoscalar coupling contributing to the  $\pi_{L2}$  decay is

$$f_p = (-0.0061 \pm 0.0057) f_{\pi m_e} \quad (16)$$

Pseudoscalar currents arise in many extensions of the standard model.<sup>9</sup> In many models with charged Higg's particles, the Yukawa coupling between the Higgs and the fermions is simply proportional to a heavy fermion mass, e.g.  $M_t$ . Using the formulation of Shanker,<sup>9</sup> a lower mass bound for charged Higgs particles resulting from the present experiment is  $M_{H^\pm} > 350$  GeV assuming maximal couplings. However, the  $\pi \rightarrow e\nu$  branching ratio is not affected for charged Higgs-fermion coupling proportional to the lepton mass as in the standard model. Other mass bounds can be set for pseudoscalar leptoquarks (>700 GeV) which occur in models with dynamical symmetry breaking such as hypercolor theories, and for vector leptoquarks (>90 TeV) in the Pati-Salam type of grand unified theories.<sup>9</sup>

#### Acknowledgements

We wish to thank G. Mason, W. Sperry and D. Berghofer for their participation in an early phase of this work and C.K. Hargrove, H. Fearing and C.E. Picciotto for many helpful discussions. We wish to thank J. Ng for his encouragement and helpful discussions and B.C. Robertson for his participation in the data-taking phase of this work. The experiment was funded in part by the Natural Sciences and Engineering Research Council of Canada.

#### FOOTNOTES AND REFERENCES

- \*TRIUMF and University of Victoria, Victoria, B.C., Canada  
 †National Research Council of Canada  
 ‡TRIUMF and University of Victoria;  
 mailing address: SLAC, Stanford CA 94305  
 §TRIUMF  
 ¶TRIUMF and University of Victoria;  
 present address: University of Ife, Ile-Ife, Nigeria  
 ||TRIUMF and University of British Columbia, Vancouver, B.C., Canada  
 1M. Ruderman and R. Finkelstein, Phys. Rev. 76 (1949) 1458.  
 2T. Fazzini et al., Phys. Rev. Lett. 1 (1958) 247.  
 G. Impeduglia et al., Phys. Rev. Lett. 1 (1958) 249.  
 3W.J. Marciano and A. Sirlin, Phys. Rev. Lett. 36 (1976) 1425.  
 See also D.A. Bryman, P. Depommier and C. Leroy, Physics Reports 88, (1982) 153.  
 4S.M. Berman, Phys. Rev. Lett. 1 (1958) 468.  
 5T. Kinoshita, Phys. Rev. Lett. 2 (1959) 477.  
 6T. Goldman and W.J. Wilson, Phys. Rev. D15 (1977) 709.  
 7J.A. Jaros et al., Phys. Rev. Lett. 51 (1983) 955.  
 8M. Kobayashi and T. Maskawa, Prog. Theor. Phys. 49 (1973) 652.  
 9H.E. Haber, G.L. Kane and T. Sterling, Nucl. Phys. B161 (1979) 493;  
 J.F. Donoghue and L-F. Li, Phys. Rev. D19 (1979) 945;  
 B. McWilliams and L-F. Li, Nucl. Phys. B179 (1981) 62;  
 O. Shanker, Nucl. Phys. B204 (1982) 375;  
 K. Mursula, M. Roos and F. Scheck, Nucl. Phys. B219 (1983) 321.  
 10R.E. Shrock, Phys. Rev. D24 (1981) 1232.  
 11D.A. Bryman et al., Phys. Rev. Lett. 50 (1983) 1546.

- <sup>12</sup>H.L. Anderson et al., Phys. Rev. 119 (1960) 2050.  
<sup>13</sup>E. Di Capua et al., Phys. Rev. 133 (1964) B1333  
<sup>14</sup>D. Bryman and C. Picciotto, Phys. Rev. D11 (1975) 1337.  
<sup>15</sup>D.A. Bryman et al., Phys. Rev. Lett. 50 (1983) 7.  
<sup>16</sup>K. Nagata, Nucl. Instr. and Meth. 77 (1970) 218.  
<sup>17</sup>S.G. Brown and S.A. Bludman, Phys. Rev. B136 (1964) 1160.  
<sup>18</sup>C. Fronsdaal and H. Uberall, Phys. Rev. 113 (1959) 654. See also  
G. Kallen, Springer Tracts in Mod. Physics 46 (1968) 67.  
<sup>19</sup>H.A. Bethe, Phys. Rev. 89 (1953) 1256. See also W.T. Scott, Rev.  
Mod. Phys. 35 (1963) 231.  
<sup>20</sup>A.O. Hanson et al., Phys. Rev. 84 (1951) 634.  
<sup>21</sup>W. Heitler, Quantum Theory of Radiation, Clarendon Press, Oxford, 1954.  
<sup>22</sup>Particle Data Group: Review of Particle Properties, Rev. Mod. Phys. 56  
(1984) S91.

<sup>23</sup>F. James and M. Roos, "MINUIT," CERN Report DD/75/20 (1975).

<sup>24</sup>Since there are theoretical uncertainties in the pion structure dependent radiative corrections, their effect is not included in the experimental and theoretical branching ratios quoted in the text. Using the conserved vector current hypothesis, the rate for the structure dependent  $\pi \rightarrow e\nu\gamma$  process has been parametrized (see Ref. 3) in terms of the  $\pi^0$  lifetime and  $h$ , the ratio between the vector and the axial vector pion weak form factors. At present, there are two possible experimental values of  $h$ ,  $-2.36 \pm 0.12$  and  $0.44 \pm 0.12$ . For  $h = -2.36$  the theoretical expectation of Eq. (1) would become  $R_{\text{theory}} = 1.238 \times 10^{-4}$  and the experimental result would be increased to  $R_{\text{exp}} = (1.223 \pm 0.014) \times 10^{-4}$  to take account of unobserved events with  $E_e < 51$  MeV due to the structure

dependent radiation. For  $h = 0.44$ ,  $R_{\text{theory}} = 1.234 \times 10^{-4}$  and  $R_{\text{exp}} = (1.218 \pm 0.014) \times 10^{-4}$ . Thus the difference between the theory and the experiment remains unaltered.

Table I

Counter Dimensions in the  $\pi$ ev Experiment (see Fig. 1)  
(horizontal $\times$ vertical $\times$ thickness in mm)

Beam Scintillators  
 B1 and B2: 30.0 $\times$ 30.0 $\times$ 9.5  
 B3, B4, B5, B6 and B7: 76.2 $\times$ 50.8 $\times$ 1.6  
 B3A, B7A: 8.4 $\times$ 50.8 $\times$ 1.6  
 B8: 305 $\times$ 305 $\times$ 3.2  
 Trigger Scintillators  
 T1: 50.8 diameter $\times$ 1.6 or 76.2 diameter $\times$ 1.6  
 T2: 483 $\times$ 483 $\times$ 3.2  
 T3: 127 diameter $\times$ 1.6

Multiwire Proportional Chambers

MWPC1: 203 $\times$ 203  
 MWPC2 and MWPC3: 305 $\times$ 305

Table II

Monte Carlo fits to the  $\pi \rightarrow e\nu$  data,  $\mu \rightarrow e\nu\bar{\nu}$  decay spectrum,  
low energy peaks and the energy calibration.

Quantity	Calibrated Energy (MeV)	Monte Carlo Energy (MeV)	$\Delta E$ (MeV)
$\pi \rightarrow e\nu$ Peak	65.90	65.88	0.020
$\pi \rightarrow e\nu$ Width	3.36	3.43	-0.065
$\mu \rightarrow e\nu\bar{\nu}$ Peak	41.78	41.73	0.049
$\mu \rightarrow e\nu\bar{\nu}$ Width	28.63	28.46	0.169
Pedestal	0.027	0.0	0.027
$e^+e^-$ annihilation radiation	0.477	0.511	-0.034

$$E_{\text{calib}}(\text{MeV}) = -3.78 + 0.14981 \times \text{Channel}$$

Table III  
Multiplicative corrections to  $\pi + e\nu$  branching ratio  
obtained by the two bin method

$\pi + e\nu$ tail	1.0147 $\pm$ 0.0075
Low-energy $\mu + e\nu\nu$	0.9982 $\pm$ 0.0005
Multiple Coulomb scattering	0.9977 $\pm$ 0.0040
Positron annihilation	0.9959 $\pm$ 0.0010
Bin 1 and bin 2 equality	0.9989 $\pm$ 0.0004
Pileup correction	0.9931 $\pm$ 0.0029
Pion lifetime	1.0000 $\pm$ 0.0009
Pion-muon solid angle difference	0.9986 $\pm$ 0.0011
$\pi$ - $\mu$ decay false veto in target	1.0002 $\pm$ 0.0010
Positron false veto in target (B7 1lp)	1.0018 $\pm$ 0.0017

Table IV  
Corrections and Uncertainties for  $\pi e\nu$  Branching Ratio  
Determination from Time Spectra

Fixed Parameters in fit	Magnitude	Corresponding Uncertainty in R
Tail correction p	0.021	$\pm 0.75\%$
$\mu$ contamination in beam, $\alpha_1$	0.00	$\pm 0.06\%$
B3 false stop pileup, $\alpha_2$	-0.00475	$\pm 0.3\%$
Stop pileup inefficiency, $\alpha_3$	0.00024	$< 0.1\%$
Positron false veto in target (B7 1lp)	0.999, (-7 $\sqrt{t}$ >7) ns	$< 0.1\%$
TINA pileup	1.000, (-7 $\sqrt{t}$ >7) ns	$\pm 0.06\%$
	1-0.004e $^{-\lambda_{\mu} t}$ ;	
	( $\pi$ - $\mu$ -e, $\pi e$ ) $^{\pm}$	
	1+0.03e $^{-\lambda_{\mu} t}$ ;	
	(muons)	
<u>Multiplicative Corrections to R</u>		
Low energy $\mu + e\nu\nu$ loss	0.9982	$\pm 0.05\%$
Pion-muon solid angle difference	0.9986	$\pm 0.11\%$
$\pi + \nu e$ decay false veto in target	1.0002	$\pm 0.10\%$
Multiple Coulomb scattering	0.9977	$\pm 0.40\%$
Positron annihilation	0.9959	$\pm 0.10\%$
<u>Fitting Procedure</u>		
Anomalous distortion at $\sim 120$ ns		$\pm 0.10\%$
Fitting region included		$\pm 0.30\%$
Unknown background		$\pm 0.30\%$



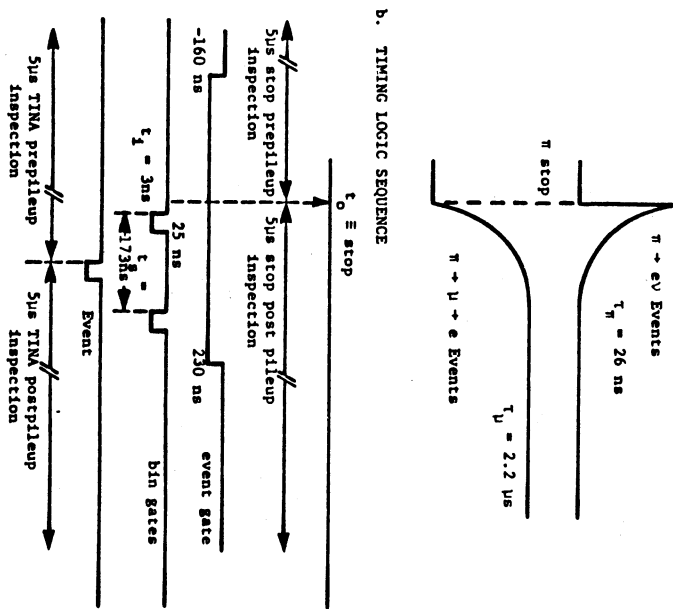


Fig. 3

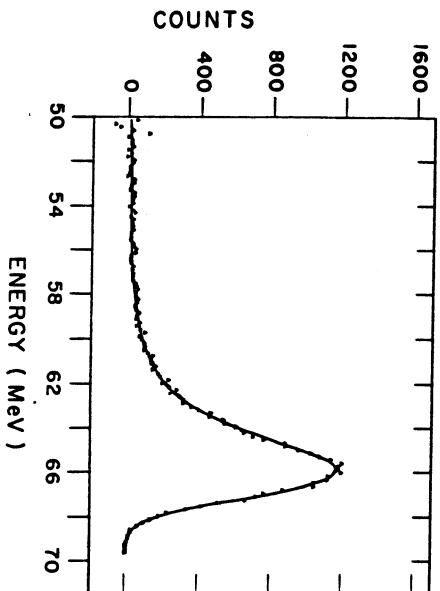


Fig. 6

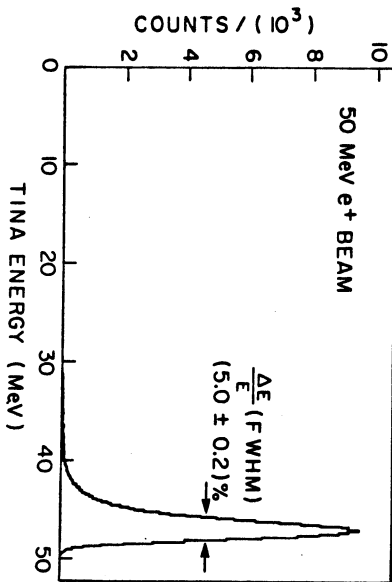


Fig. 4

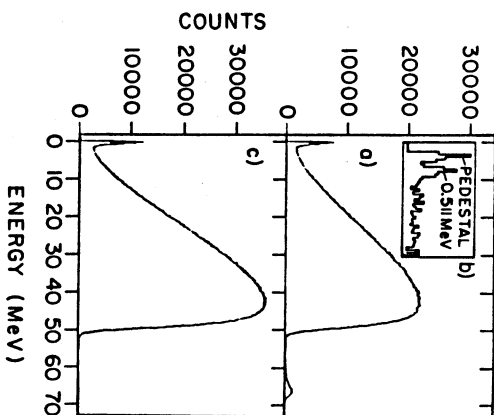


Fig. 5

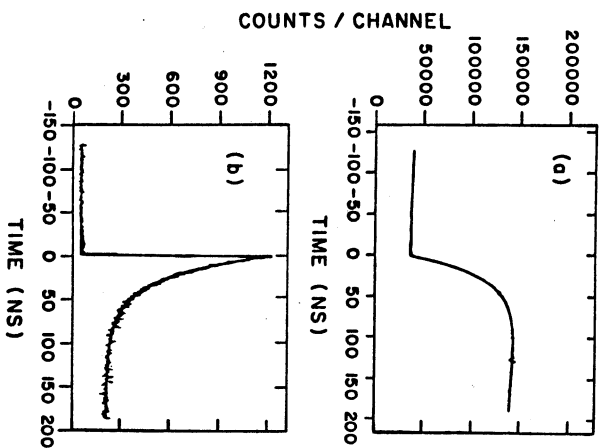


Fig. 7

Figure Captions

- [1] Experimental set-up with details of the stopping counter sandwich B3-B7 (inset).
- [2] Schematic of a) stop logic, b) event logic, and c) pileup logic.
- [3] a) Event time distribution with respect to the pion stop.  
b) Logic time sequence for event with respect to the pion stop.
- [4] Measured line shape in the NaI(Tl) crystal TINA for 50 MeV  $e^+e^-$  beam.

The position of the peak (47.2 MeV) is determined by energy loss in the beam scintillators and the insensitive layer in front of the TINA crystal as well as positron annihilation.

- [5] a) Positron energy spectrum for events in Bin 1.  
b) Expanded scale low energy region for Bin 1.  
c) Positron energy spectrum for events in Bin 2.
- [6] Fit to the  $\pi \rightarrow e\nu$  line with the Monte Carlo generated line shape.
- [7] Time distribution for a) events below  $E_C=52.9$  MeV and b) events above  $E_C$ . Solid lines are fits to the data.

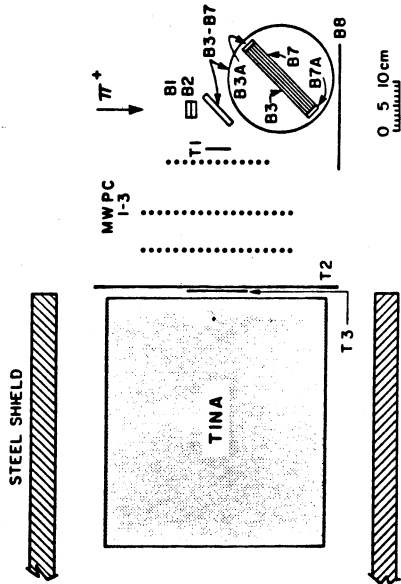
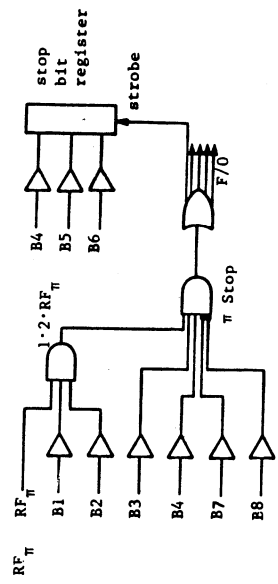
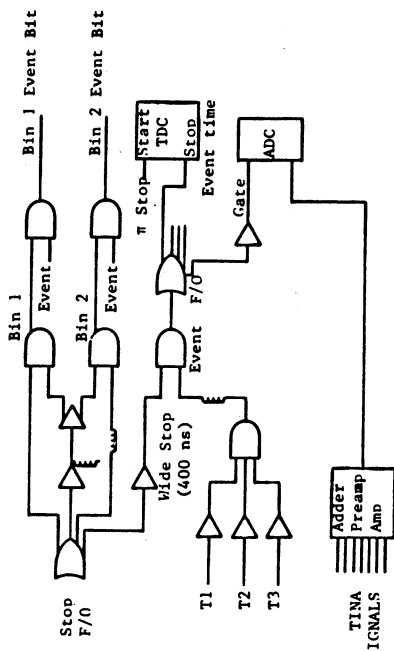


Fig. 1

a. STOP LOGIC



b. EVENT LOGIC



c. PILEUP LOGIC

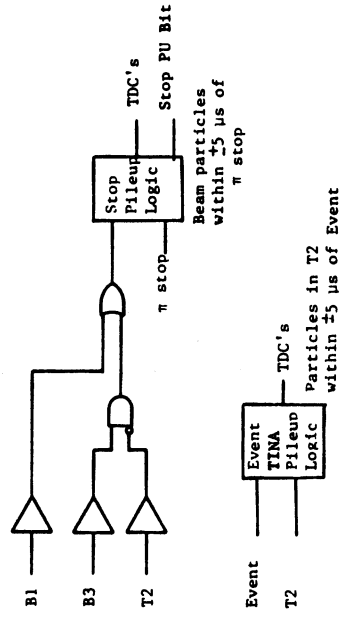


Fig. 2